



Microstructure, Mechanical Properties and Fretting Wear Behavior of Gravity Die Cast and Squeeze Cast AZ91 Mg Alloy

Ankush S. Marodkar¹ · Hitesh Patil¹ · Hemant Borkar¹

Received: 22 January 2023 / Revised: 22 April 2023 / Accepted: 10 May 2023 / Published online: 26 May 2023
© ASM International 2023

Abstract

In the present work, the change in microstructure and mechanical properties of squeeze cast (SC) AZ91 Mg alloy has been studied by comparing it with conventional gravity die-cast (GC) AZ91 alloy. The present study also focuses on the effect of microstructure change in GC and SC AZ91 samples on the fretting wear behavior. The fretting wear studies are conducted on GC and SC AZ91 samples against the EN31 steel pin by variation in applied loads (5, 10, 15 N) and oscillating frequencies (5, 10, 15 Hz). SC AZ91 alloy exhibits improved tensile properties than that of GC AZ91 due to refined microstructure. The study demonstrates that the average coefficient of friction decreases with an increase in normal load and increases with an increase in frequency for both GC and SC AZ91. The wear volume loss is found to increase with an increase in applied load and frequency. It is proposed that the wear in GC and SC AZ91 alloy is caused by a combination of adhesion, oxidation, delamination, and abrasion under different fretting conditions. For every condition studied in the present work, the SC AZ91 exhibits better fretting wear resistance compared to GC AZ91.

Keywords AZ91-magnesium alloy · Squeeze casting · Mechanical properties · Tribology · Fretting wear

Introduction

Magnesium-based alloys are employed in the automotive, aviation, and military industries due to its low density, high specific strength, superior castability and machinability, and strong damping properties [1, 2]. However, because of the limited slip systems caused by the HCP crystal structure, processing Mg alloys becomes challenging [3, 4]. AZ91, an Al–Zn based Mg alloy with outstanding casting qualities and good corrosion resistance at a reasonable cost, is one of the most extensively used Mg alloys in the automotive industry [5, 6]. The microstructure of AZ91 consists of two phases, α -Mg (α -phase) and β -Mg₁₇Al₁₂ (β -phase). When AZ91 is processed by gravity die casting, the grain boundaries (GBs) are largely occupied by the β -phase. Hence β -phase, being a brittle phase, negatively affects the alloy's mechanical properties by serving as an intercrystalline cracking site [7, 8]. β -phase, with its low thermal stability,

is susceptible to softening as a result of frictional heating at the surface, increasing the wear rate [9]. The refinement of microstructure through alloying is a commonly employed method to enhance the mechanical properties of the AZ91 alloy [10, 11]. In addition to alloying, hot forming processes forging, rolling extrusion, etc., are being used for further enhancement of mechanical properties of the AZ91 alloy [12, 13]. Apart from this, the different alloy making route could enhance the mechanical properties of the AZ91. The squeeze casting method can overcome the negative effects of β -phase in AZ91 to some extent. The squeeze casting technique produces a fine and consistent β -phase network, which may improve the mechanical and wear properties of the AZ91 alloy [8]. Previous research on squeeze cast Mg alloys revealed both continuous and discontinuous β -phase precipitates [14–16].

The majority of components used in industrial applications are vulnerable to wear, hence studying tribological properties of material has become a significant topic of study. Components such as gears, bearings, clutches, spines, and so on are subjected to small amplitude quasi-static point contact loading conditions and, as a result, fretting-induced damages [17].

✉ Hemant Borkar
h.borkar@iiti.ac.in

¹ Department of Metallurgy Engineering and Materials Science, Indian Institute of Technology Indore, Khandwa Road, Simrol, Indore, Madhya Pradesh 453552, India

Steel rivets and bolts are commonly used to fasten structural pieces manufactured of AZ91 in cars and aircrafts. These components are subjected to low-amplitude oscillatory motion, resulting in fretting wear conditions [18]. The cast AZ91 alloy is mainly used in automobiles to prepare power train components. Additionally, AZ91 is utilized to manufacture automobile parts like cross-car beams, brackets, battery covers, sheet frames, electronic control unit (ECU) casings, etc. that may experience severe wear over time as a result of automobile vibrations. In addition, the components must be connected to form a useful component for aerospace and automotive applications. For such purposes, arc welding of Mg-based alloys may not be a viable alternative due to their flammable nature. As a result, one of the practical alternatives is to rivet or bolt joints. However, because of the clearance between the surfaces, mechanical attaching does cause relative motion on a micrometer-length scale. Damage caused by relative motion on a micrometer length scale, or fretting, cannot be disregarded and poses a major safety risk. Fretting wear is surface damage that develops between two surfaces of contact under the action of applied normal load and experiences an oscillatory tangential displacement or cyclic motion of small amplitude (in the range from nanometer to 200 μm). Assessment of fretting-induced wear is crucial for determining the safe service life of components subjected to engineering applications since fretting may enhance vibration/damping or cause the component under service to fail catastrophically [19–23].

Abrasive, adhesive, and oxidative wear mechanisms are generally responsible for fretting wear. There are several fretting wear regimes, including as gross slip, partial slip, and stick–slip regimes, which represent the morphology of wear scar [18, 24]. Some industrial components that are subjected to fretting wear include valve-to-valve seat interfaces, bearings, rivet joints, and gas turbine combustor components.

Very few studies are available in the literature on fretting wear behavior of Mg alloys. Khabale et al. [20] investigated fretting wear of AZ91 and AE42 alloys against steel ball as the counter surface. According to their findings, the amount of wear and the wear processes varied depending on the contact conditions, the type of regime, and the applied normal load used at a specific fretting wear frequency. However, they found that the average coefficient of friction increased moderately with increasing fretting amplitude and reduced with increasing load applied and frequency. They also found that AZ91 alloy has better wear resistance than AE42 alloy. They revealed that surface conditions had a significant influence in the wear of both alloys at higher frequencies, and that the oxidation layer reduced the coefficient of friction. The main wear processes that take place during fretting wear of AZ91/steel and AE42/steel tribopair include adhesion, oxidation, abrasion, plastic deformation, and delamination.

Huang Weijiu et al. [21] investigated the fretting wear behavior of AZ91D and AM60B alloys. Abrasion, adhesion, and surface fatigue wear were discovered to be common fretting wear processes for both alloys. Additionally, compared to AM60B alloy, AZ91D had a lower coefficient of friction and reduced wear volume loss. Koushik Sikdar et al. [24] investigated the fretting wear of the Mg–Li–Al-based alloys LATZ9531 and LAT971. The fretting wear parameters that were varied are the number of fretting cycles ($10\text{--}10^4$), normal load (1–10 N), oscillation frequency (1–9 Hz), and displacement amplitude (80–200 μm). They discovered that when the fretting frequency increased, a third body, an oxide layer, became a part of the wear and helped to lower the coefficient of friction. Additionally, they came to the conclusion that, surface asperities quickly reach a stable state as the normal load increased by equilibrating with the loading ball, thereby lowering the mean coefficient of friction.

Fretting is one of the most damaging issues for modern industry and can cause serious localized wear of the emerging AZ91 Mg alloy components. However, the fretting wear study of Mg alloy is very limited, especially for AZ91. The change in microstructure by changing the casting process could affect the mechanical and wear behavior of the AZ91 alloy. The effect of microstructure change on fretting wear behavior of AZ91 alloy following the squeeze casting method has not yet been studied. Accordingly, the current work first focuses on the effect of the squeeze casting method on the microstructure and mechanical properties of AZ91 alloy. Furthermore, an attempt has been made to study the effect of the squeeze casting process on the fretting wear behavior of AZ91 alloy. The fretting wear tests and analysis of wear mechanisms have been carried out on varying oscillating frequencies and varying loading conditions. The obtained results of squeeze cast sample have been compared with those of conventional gravity die-cast AZ91 sample.

Experimental Procedure

Casting of Alloy Sample

The alloys used in this work were cast by the re-melting of commercial AZ91 Mg alloy. Both gravity die-cast (GC) and squeeze cast (SC) AZ91 alloy were prepared using Swam-Equip's bottom pouring type stir casting equipment. To prevent oxidation, the melting was carried out in a graphite crucible at 700 °C in an Ar (99.5 vol.%) + SF₆ (0.5 vol.%) environment. After the complete melting of the AZ91 blocks in the crucible, the melt was poured into the cylindrical mold through the bottom pouring arrangement to prepare the gravity die-cast sample. To prepare the squeeze cast sample, the poured melt in the mold was squeezed at 100 MPa pressure for 60 s immediately after pouring [5, 14, 25]. The surface

of the mold was coated with a thin graphite oil layer and preheated up to 200 °C by utilizing an external heater before pouring the melt. The chemical compositions of the obtained GC and SC AZ91 rod sample are given in Table 1.

Microstructure and Phase Analysis

The obtained GC and SC AZ91 rods were cut by using wire-cut electrical discharge machining. For microstructure analysis, 10 × 10 mm samples of GC and SC AZ91 billets were polished by using 100 to 2000 grades of emery paper before the cloth polishing with 9 to 1 micron diamond suspension. After fine polishing, the samples were etched by using an acetic picral solution (100 mL Ethanol, 6 g Picric acid, 5 mL Acetic acid, 20 mL DI Water) for 1–2 s. The microstructure images of the etched sample were obtained from ZEISS Axio Vert. A1 inverted optical microscope (OM) and JEOL JSM-7610 F plus field emission scanning electron microscopy (FE-SEM). The grain size was measured using the electron backscattered diffraction (EBSD) technique. To analyze the phases, present in the GC and SC castings, the x-ray diffraction (XRD) pattern was obtained by using PAN analytical X'Pert High Score x-ray diffractometer employing CuK α ($\lambda = 1.541 \text{ \AA}$) radiation. Using ImageJ software, the secondary dendrite arm spacing (SDAS) in the produced GC and SC AZ91 alloys were measured from FE-SEM images of five different locations of the test samples (GC and SC AZ91).

Microhardness and Tensile Testing

The microhardness of both samples (GC and SC AZ91) was determined by using a Mitutoyo Co. HM 112 Micro Vickers hardness tester at 300 g load and 20 s dwell time. The polished and etched sample was indented five times, and the average hardness value was calculated.

The tensile testing was performed using a Instron 5967 Universal tensile testing machine (UTM). The subsize tensile specimens were used for tensile testing following the ASTM E8 standard. The sample dimensions for tensile testing are shown in Fig. 1. The three specimen were taken from each fabricated alloy for testing and the average values of tensile properties were measured. The tensile tests were performed at a 0.001 s⁻¹ strain rate and 28 °C temperature (room temperature).

Fretting Wear Test and Characterization

A Ducom fretting wear tester was used to perform fretting tests on the GC and SC AZ91 samples under various conditions, i.e., with varying load (5, 10, 15 N) and varying oscillating frequency (5, 10, 15 Hz) at room temperature. All measurements were conducted with a 200 μm vibration amplitude and 15 min time. The tests were carried out using a hardened steel grade EN31 pin with a diameter of 6 mm and a tip diameter of 2 mm with a rounded tip for point contact and a hardness of 698 HV. Figure 2a, b shows the fretting wear apparatus with a 3-D depiction of pin-to-sample contact and associated dimensional measurements. Three repetitions of each test were performed, and average results were calculated. Using the suitable equation developed by Hallings [23, 26], the wear scar volume loss (v) at room temperature for all combinations of various loads and frequencies was determined from the observed wear scar diameter.

$$v = \pi R h^2 \left(1 - \frac{h}{4R}\right)^4 \quad (1)$$

where h is the maximum wear scar depth and R is the tip radius of the pin. The maximum depth of the wear scar, h , was calculated from the measured mean wear scar diameter, d , using the relations:

$$h = R - \left(R - \frac{d^2}{4}\right)^{1/2} \quad (2)$$

$$d = \frac{d_{\parallel} + d_{\perp}}{2} \quad (3)$$

The wear scar depth and measurement of wear scar diameter on plate in parallel (d_{\parallel}) and perpendicular (d_{\perp}) direction to fretting movement are illustrated in Fig. 2c. The wear scar volume was calculated using an average of at least three measured wear scar diameter values from FESEM images of wear scar. The micro-mechanisms of fretting wear damage were studied

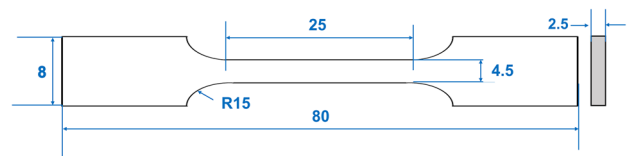


Fig. 1 Tensile test specimen (all dimensions are in mm)

Table 1 Chemical composition (in wt.%) of gravity die-cast (GC) and squeeze cast (SC) AZ91 Mg alloy

Alloy	Chemical composition, wt.%								
	Al	Zn	Mn	Si	Fe	Cu	Ni	Sn	Mg
GC AZ91	9.01	1.57	0.17	0.022	0.009	0.006	0.003	0.003	Bal.
SC AZ91	9.15	1.49	0.16	0.021	0.008	0.006	0.004	0.002	Bal.

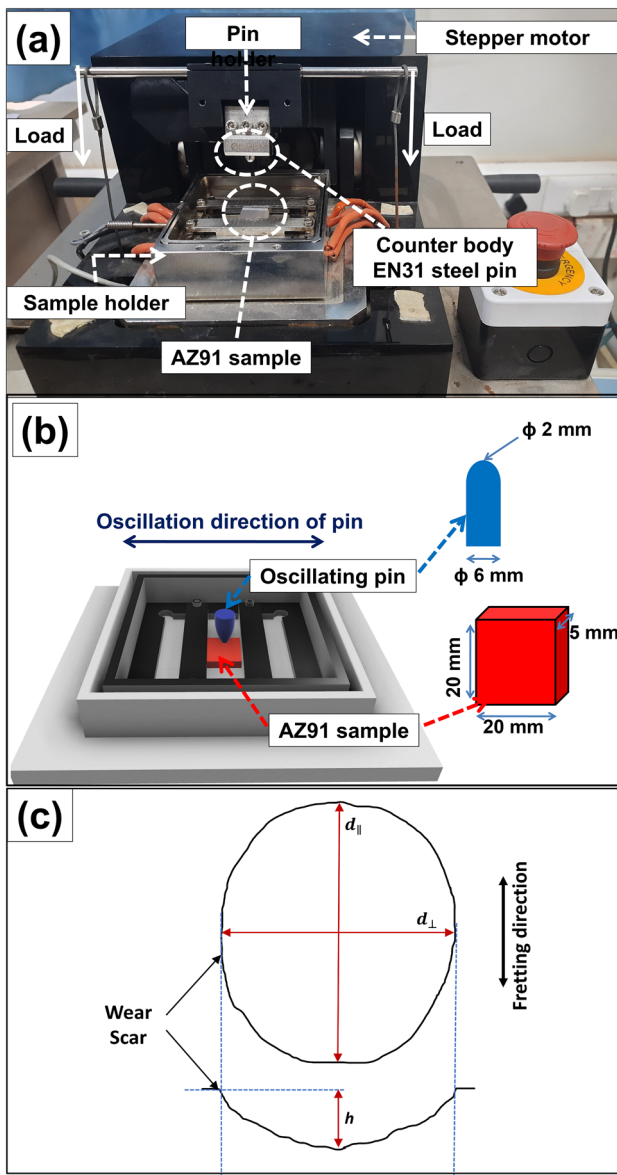


Fig. 2 (a) Fretting wear apparatus with (b) a 3D representation of pin-to-sample contact with their dimensional measurements, and (c) schematic representation of wear scar diameter and maximum wear scar depth, h

using a FE-SEM microscope. The elemental mapping of wear scars were carried out by using energy dispersive spectroscopy (EDS) facility available in FE-SEM.

Results and Discussion

Phase Analysis and Microstructure Characterization of Gravity Die-Cast (GC) and Squeeze Cast (SC) AZ91 Alloy

Figure 3 shows the XRD graphs of GC and SC AZ91 Mg alloy. In both alloys (GC and SC AZ91), the XRD graph

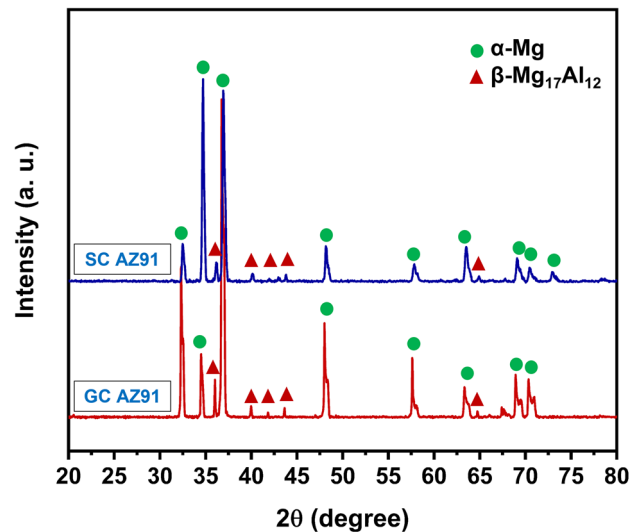


Fig. 3 XRD analysis of GC and SC AZ91 Mg alloy

demonstrates the existence of the α -Mg matrix as the major phase and the β -Mg₁₇Al₁₂ (β -phase) as the secondary phase. The morphologies of the α -Mg and β -phase are further observed by the microstructure analysis in Fig. 4.

Figure 4 shows the optical, FESEM, and EBSD micrographs of GC and SC AZ91 alloy. The optical and FESEM images show the presence of the α -Mg phase as the matrix and the semicontinuous interdendritic network of β -Mg₁₇Al₁₂ (β -phase) in the α -Mg matrix. In each alloy, the secondary β -phase is distributed differently. In Fig. 4a, the GC AZ91 micrograph shows unpreventable casting defects like porosity and segregation defects, and they might act as the possible crack nucleation site for material damage [27]. In contrast, squeeze casting results in a fine, homogenous microstructure with nearly little porosity and fewer casting defects (Fig. 4d). The outcomes of this research work on squeeze cast samples are consistent with the other studies that have previously been published for squeeze castings of Mg–Al alloys [28–30]. The SC AZ91 alloy (Fig. 4e) reveals the existence of refined, more joint and continuous interdendritic network of β -Mg₁₇Al₁₂ precipitates while the GC AZ91 alloy (Fig. 4b) has segregated blocks of β -Mg₁₇Al₁₂. Prior research on squeeze casting of magnesium alloys has also noted such microstructure refinement of β -phase after squeeze casting [31–34]. During squeeze casting, nonequilibrium solidification of molten metal occurs due to applied pressure. Hence, the higher solidification rate in the squeeze casting process is responsible for the refine and homogeneous distribution of the secondary interdendritic network of the β -phase [33]. The secondary dendrite arm spacing (SDAS) was measured from the optical images of GC and SC AZ91 from 5 different locations in each alloy, and the measured values

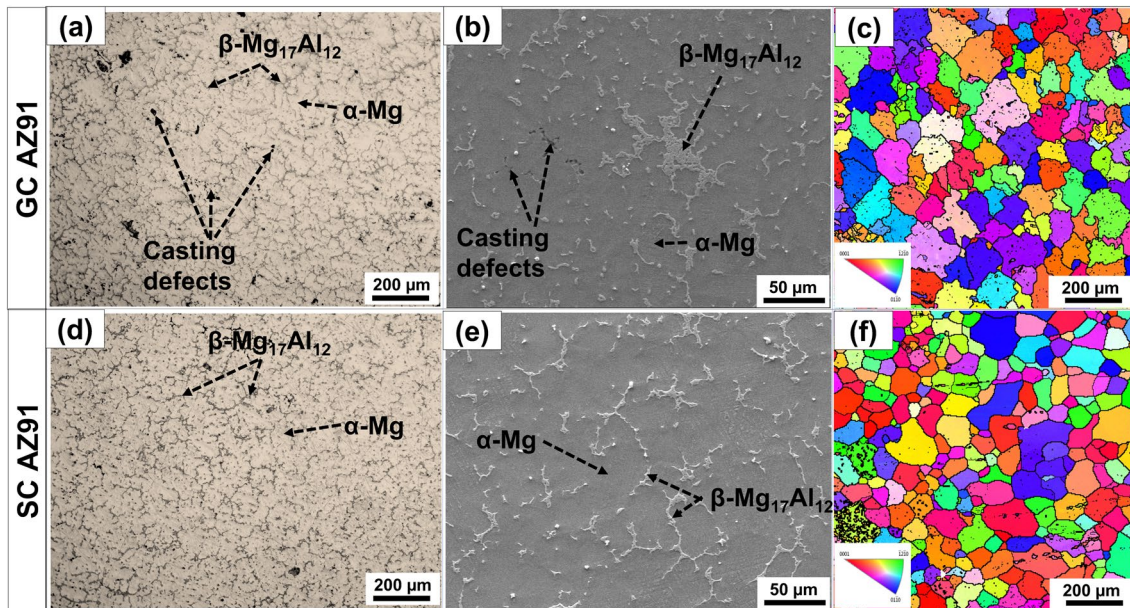


Fig. 4 (a) Optical micrograph, (b) FESEM image, and (c) EBSD map of GC AZ91; (d) optical micrograph, (e) FESEM image, and (f) EBSD map of SC AZ91

Table 2 Calculated values of secondary dendrite arm spacing (SDAS) and average grain size (AGS) of GC and SC AZ91 alloys

Alloy	SDAS, μm	AGS, μm
GC AZ91	91 ± 9	79 ± 5
SC AZ91	69 ± 8	58 ± 4

are tabulated in Table 2. It can be noted that the SDAS value of the SC AZ91 is lower by 24.13% than that of GC AZ91. As the secondary dendritic network mostly forms at the surface of α -Mg grains surface, the reduction in SDAS value in the squeeze casting process could result in the reduction in the average grain size (AGS) of squeeze cast alloy. The EBSD maps of GC and SC AZ91 are presented in Fig. 4c and f, respectively, and AGS values are tabulated in Table 2. Due to higher solidification rates achieved in squeeze casting process, SC AZ91 sample was found to have 26.58% lower AGS than that of GC AZ91 sample.

Microhardness Measurements of GC and SC AZ91 Alloy

The measured average Vickers's hardness value of GC AZ91 alloy and SC AZ91 alloy are 74 ± 10 HV and 81 ± 9 HV, respectively. The improvement in hardness value of the sample after squeeze casting is the result of the increase in grain boundary density and formation of a continuous network of

β - $\text{Mg}_{17}\text{Al}_{12}$ which provides a higher resistance to penetration of indenter. The increased hardness following the squeeze casting is also expected to lead to an improvement in wear resistance [35].

Mechanical Properties of GC and SC AZ91 Alloy

The measured tensile properties of GC AZ91 and SC AZ91 samples are plotted in Fig. 5 and tabulated in Table 3. The data shows that the squeeze cast samples demonstrate better tensile properties than that of gravity die cast samples. Tensile yield stress (TYS), ultimate tensile stress (UTS), and

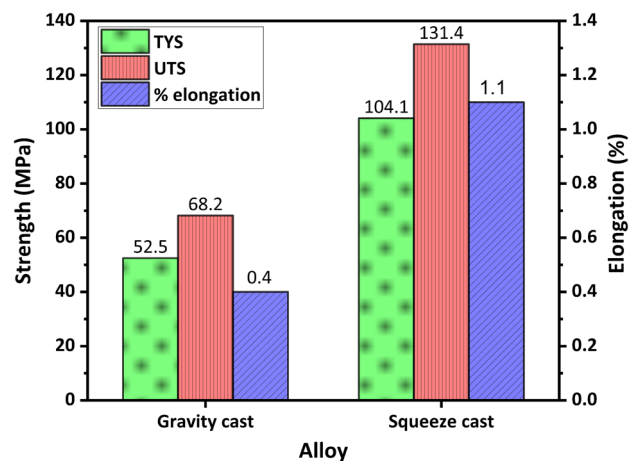


Fig. 5 Tensile properties of gravity cast and squeeze cast AZ91 alloy (TYS—tensile yield stress, UTS—ultimate tensile stress)

Table 3 Tensile properties of GC and SC AZ91 Mg alloys

Alloy	Tensile properties		
	TYS, MPa	UTS, MPa	Elongation, %
GC AZ91 alloy	52.5 ± 6.1	68.2 ± 9.2	0.4 ± 0.2
SC AZ91 alloy	104.1 ± 8.0	131.4 ± 10.6	1.1 ± 0.3

percent elongation were enhanced in the SC AZ91 sample by 98.28, 92.6, and 175.0%, respectively, with respect to GC AZ91 sample.

The enhanced mechanical properties of SC alloy are primarily due to two factors: Hall–Petch strengthening and a decrease in casting defects. The reduced grain size and refined β -phase network in SC AZ91 alloy (Fig. 4) are caused by the faster solidification of the melt in the squeeze casting process [36]. The elimination of casting defects like porosity, blowholes, etc., in the SC method (Fig. 4) were discussed previously in this paper. The casting defects serve as a location for crack formation and hence degrade the mechanical strength in gravity die cast sample. Therefore, it has been established that the squeeze casting method produces superior castings compared to the gravity die-casting method.

Fretting Wear of GC and SC AZ91 Alloy

Effect of Oscillating Frequency on COF and Wear Volume Loss

The coefficient of friction is defined as the ratio of the amplitude of the tangential force to the normal load applied [24]. Figure 6 shows the variation of the average coefficient of friction with respect to oscillating frequency for GC AZ91 and SC AZ91 alloy samples. The load was varied at 5, 10, and 15 N while maintaining constant fretting amplitude (200 μm). The fretting amplitude is the distance traveled by the center of the counter body while oscillating from the initial to the final position. At all three loads, the COF values

are observed to increase with an increase in frequency from 5 to 15 Hz for both GC and SC AZ91 alloys. Increasing the velocity of relative slip increases the temperature at the contact region between the pin and the AZ91 sample. This increases oxidative wear and hence, at higher frequencies, the wear debris gets ejected rapidly from the AZ91 sample. This reduces the third body interaction between mating surfaces and the nascent surface of the test sample gets exposed to further damage. Hence, with an increase in frequency, the COF increases and consequently, severe wear may occur [24]. Considering an individual frequency, with increase in load, COF decreases. At higher loading conditions (10 and 15 N), surface asperities get strain hardened by forming their oxides. These oxides act as third-body particles to reduce the friction between the pin and AZ91 mating surfaces. Hence with an increase in applied load, the average COF decreases. For all conditions present in Fig. 6, SC AZ91 alloy samples exhibit a lower COF compared to GC AZ91 alloy.

Figure 7 indicates the FESEM images of wear scars of GC and SC AZ91 samples for different oscillating frequencies (5, 10, and 15 Hz) at a constant load (10 N) and constant amplitude (200 μm). With an increase in frequency, the GC and SC AZ91 samples elicit an increase in scar size. Such increment in wear scar size with an increase in oscillating frequency for fretting wear study of pure Niobium is also reported by Bryggman et al. [37]. Irrespective of frequency, the SC AZ91 wear scar shows a smoother and marginally lower mean diameter than the GC AZ91 sample. At 5 Hz frequency, the adhesion transfer of material is prominent in both GC and SC AZ91 alloy (by Fig. 7a and b, through appearance of adhesion grooves). Compared to the SC AZ91, at a lower frequency (5 Hz), the observed microcracks are higher in the GC AZ91 sample and lead to the cracking of the tribolayer. At higher frequencies (10 and 15 Hz), numerous cracks are observed in GC samples leading to the cracking of the tribolayer and consequently, leading to the delamination and tribo-oxidation. The delamination and oxidative wear are more dominant at higher frequencies in the GC AZ91 sample

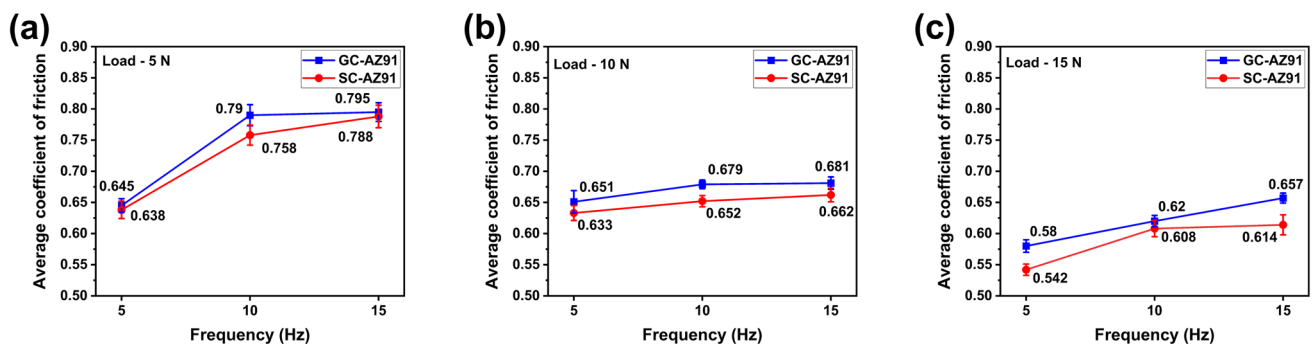


Fig. 6 Effect of oscillating frequency on the coefficient of friction at (a) 5, (b) 10, and (c) 15 N load at constant 200 μm amplitude

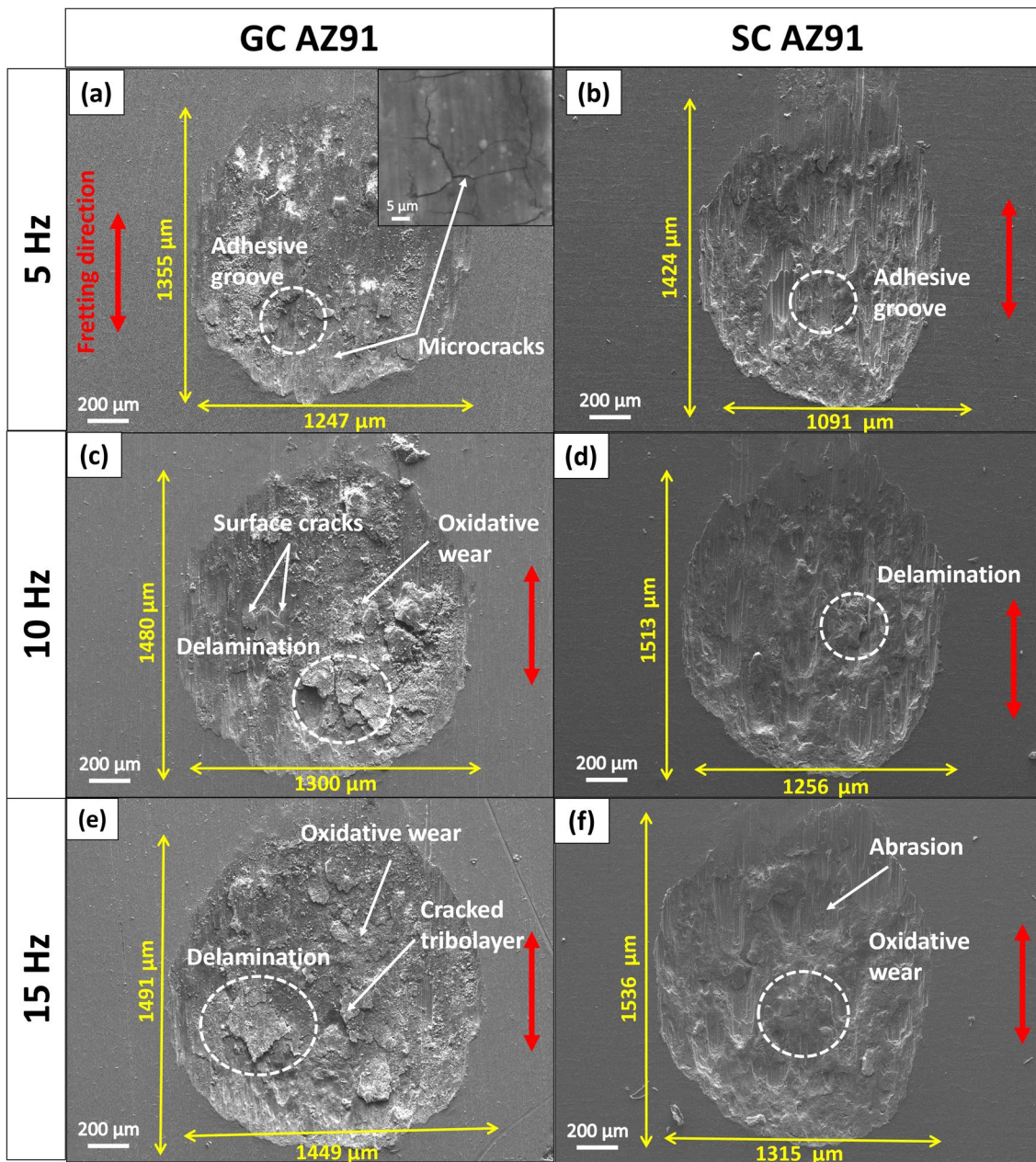


Fig. 7 FESEM images of wear scars for oscillating frequencies of (a) 5 Hz, (c) 10 Hz and (e) 15 Hz for GC AZ91 alloy and (b) 5 Hz, (d) 10 Hz and (f) 15 Hz for SC AZ91 alloy at a constant load of 10 N and constant amplitude of 200 μm

(Fig. 7c and e) compared to the SC AZ91 sample (Fig. 7d and f) which indicates severe wear of GC AZ91 samples. The amount of oxidative wear at higher frequencies in GC and SC AZ91 samples is explained further in Sect. "Effect of applied load on COF and wear volume loss".

The effect of oscillating frequency on wear volume loss at 5, 10, and 15 N load for GC and SC AZ91 samples at constant amplitude is shown in Fig. 8. At 5 and 10 N loads, the GC and SC samples show nearly similar observations. At 15 N load, with an increase in the frequency, the large

difference in wear volume can be seen in Fig. 8c. Also, at lower loads of 5 and 10 N (Fig. 8a and b), after 10 Hz frequency, the slope of the line decreases whereas, at 15 N loading condition (Fig. 8c), the slope increases drastically in 10–15 Hz range. With an increase in frequency, relative velocity in the slip zone of the contact region increases the temperature and hence oxidation takes place which results in an increase in oxidative wear (Fig. 7). Further, at a frequency of 10 Hz, the wear debris is ejected rapidly from counter surfaces and reduces third-body interferences. Hence, a

decrease in the slope of the wear volume curve was observed at a frequency from 10 to 15 Hz and at applied loads of 5 and 10 N. Whereas at higher loading conditions of 15 N, the abrasive action of hard wear debris increases the slope of the wear volume curve with an increase in oscillating frequency. In comparison with GC, SC AZ91 exhibits better wear resistance for all conditions. These wear volume results (Fig. 8) are in agreement with the COF results (Fig. 6) for both GC and SC AZ91 samples.

Effect of Applied Load on COF and Wear Volume Loss

Figure 9 shows the variation of the average coefficient of friction with respect to applied load for 5, 10, and 15 Hz oscillating frequency by keeping constant amplitude (200 μm), where GC AZ91 is compared with the SC AZ91 sample. At all three-oscillating frequencies, the average COF values are observed to decrease with an increase in load from 5 to 15 N for both GC and SC AZ91 alloys. The coefficient of friction is increases rapidly during the first few hundred cycles of fretting wear. With further increase in fretting wear cycles, the COF decreases and attains a steady state. The formation of a compact bed of oxide wear debris is responsible for attaining a steady-state COF in the later stages of the fretting wear cycle [24]. Lower loading

condition (5 N) takes a longer time to achieve a steady state in the running-in period of the tests. At higher loading conditions (10 and 15 N), surface asperities get strain hardened by forming their oxides and achieve a steady state in lesser time. These oxides act as third-body particles to reduce the friction between the pin and AZ91 mating surfaces [20, 24]. Hence with an increase in applied load, the average COF decreases. For every condition, the SC alloy shows a lower average coefficient of friction compared to the GC alloy.

Figure 10 shows the wear scar FESEM images for different loads (5, 10, and 15 Hz) at a constant oscillating frequency (10 Hz) and constant amplitude (200 μm), where the effect of loads on wear scar sizes was investigated by contrasting GC and SC AZ91 alloy. With an increase in load, the GC and SC AZ91 samples elicit an increase in wear scar size. The micro-cracks and adhesive smearing can be observed in GC AZ91 wear scar at lower loading conditions (5 N) (by Fig. 10a, through appearance of transferred smeared material in adhesive groove). GC and SC AZ91 exhibit abrasive wear tracks at low and high loads (by Fig. 10a and b, through appearance of abrasive groove). The SC sample wear scar looks smoother compared to the GC AZ91 wear scar in all loading conditions. From the wear scar images at the higher load (10 and 15 N), it is clearly visible that oxidative wear is more dominant in GC sample.

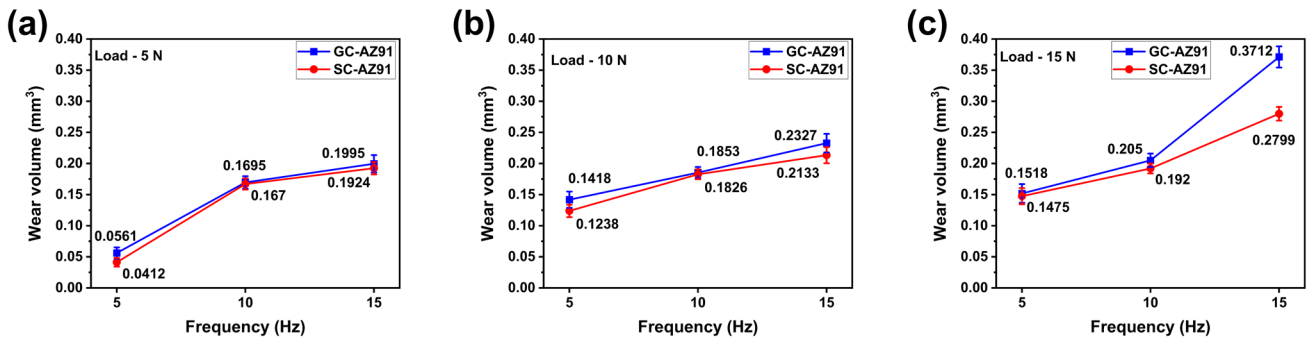


Fig. 8 Effect of oscillating frequency on the wear volume loss at (a) 5, (b) 10, and (c) 15 N load at constant 200 μm amplitude

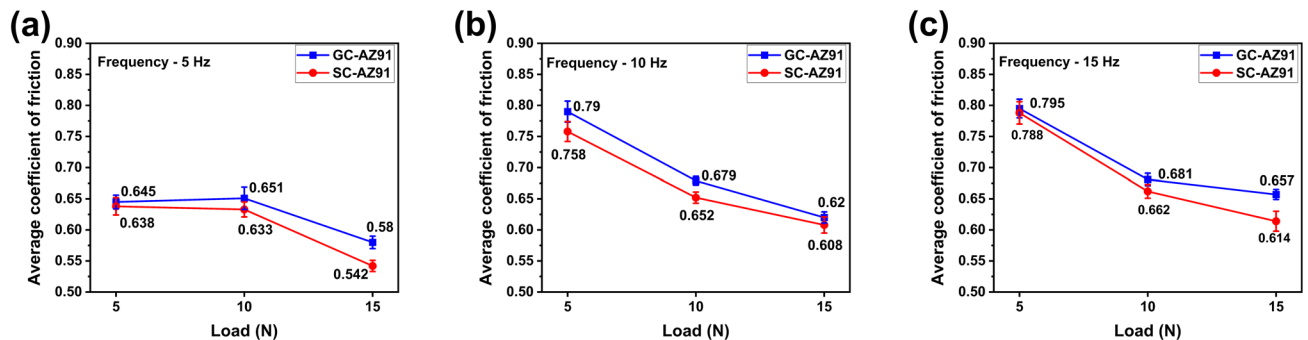


Fig. 9 Effect of load on the coefficient of friction at (a) 5, (b) 10, and (c) 15 Hz oscillating frequency at a constant 200 μm amplitude

Figure 11 shows the oxidation region is larger in the GC AZ91 sample and the SC AZ91 scar shows limited tribo-oxidation implying that the GC AZ91 sample has more oxidative wear and hence, there may be significant wear loss.

Figure 12 shows the effect of variation in loads on the wear volume loss for both the alloy samples at (a) 5 Hz, (b) 10 Hz, (c) 15 Hz oscillating frequency at a constant 200 μm amplitude. For both GC and SC AZ91 alloys in each condition, wear volume loss increases with an increase in applied normal loads. The reported wear volumes of GC and SC

AZ91 alloy did not change significantly for lower frequencies (5 and 10 Hz). At 15 Hz frequency, the tribo-oxidation is the dominant wear mechanism in GC AZ91 exhibiting higher wear volume loss compared to the SC AZ91 sample. In all conditions shown in Fig. 12, the SC sample shows a lower wear volume compared to GC Sample. From Figs. 9 and 12, it can be concluded that the coefficient of friction decreases with an increase in load but wear volume increases.

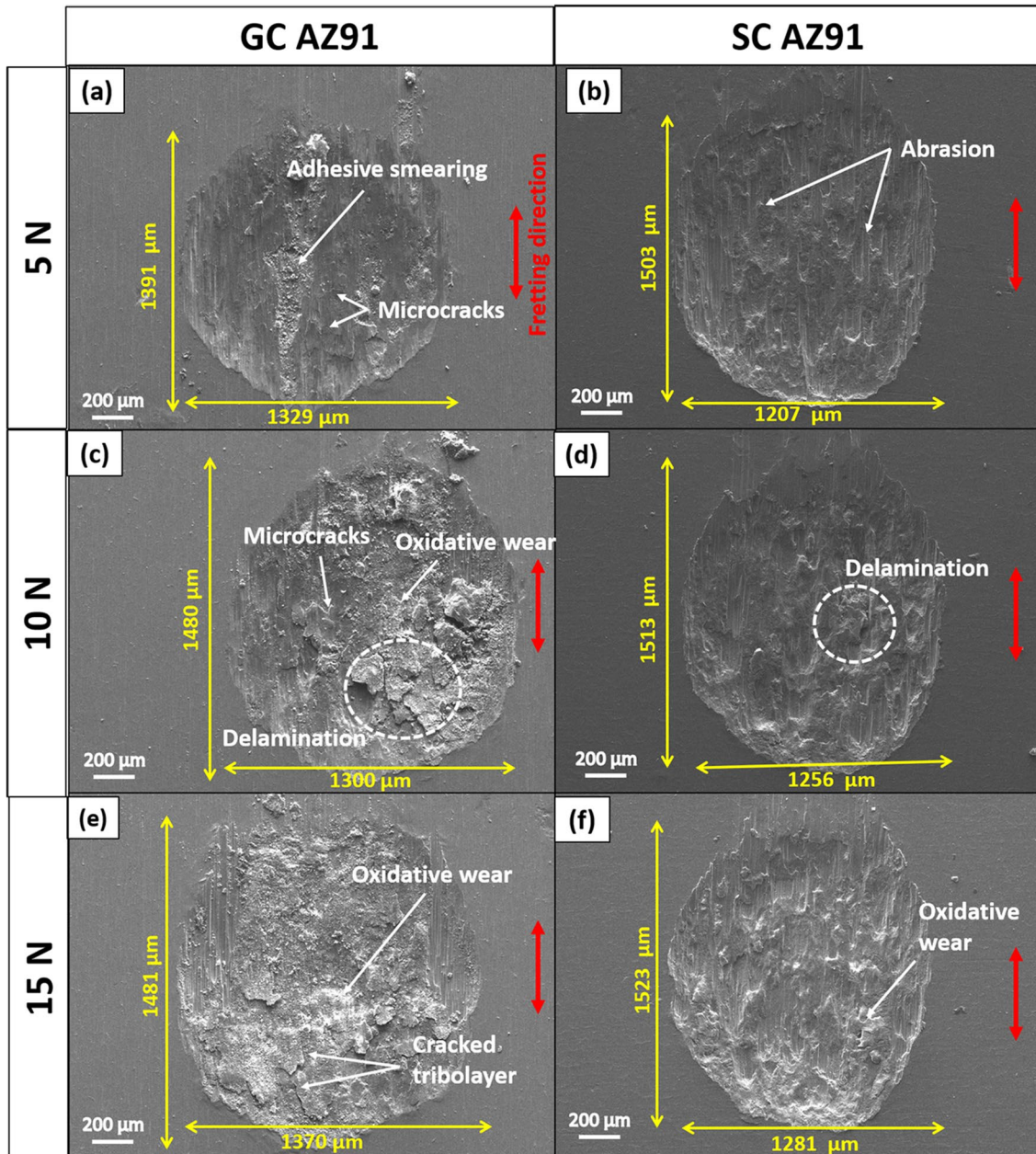


Fig. 10 FESEM images of wear scars for loading conditions of (a) 5 N, (c) 10 N and (e) 15 N for GC AZ91 alloy and (b) 5 N, (d) 10 N and (f) 15 N for SC AZ91 alloy at a constant frequency of 10 Hz and constant 200 μm amplitude

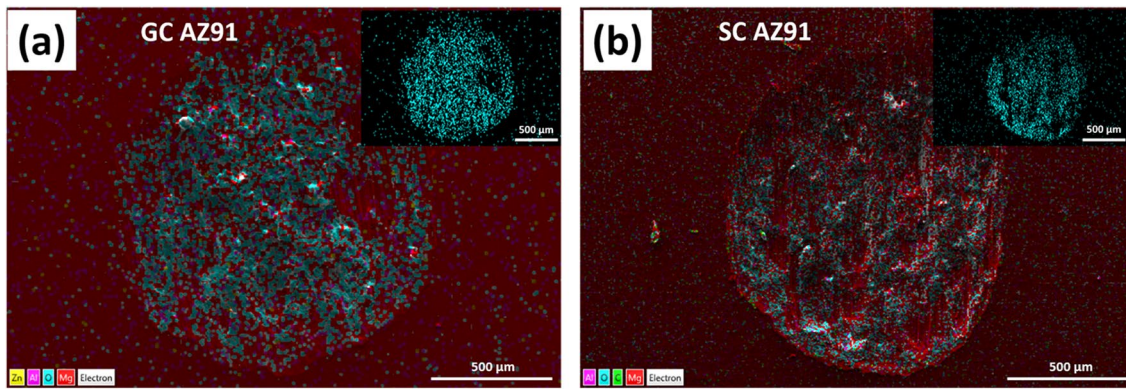


Fig. 11 Elemental mapping of (a) GC AZ91 wear scar and (b) SC AZ91 wear scar with inset showing the oxygen element map (oscillating frequency = 10 Hz and applied load = 10 N)

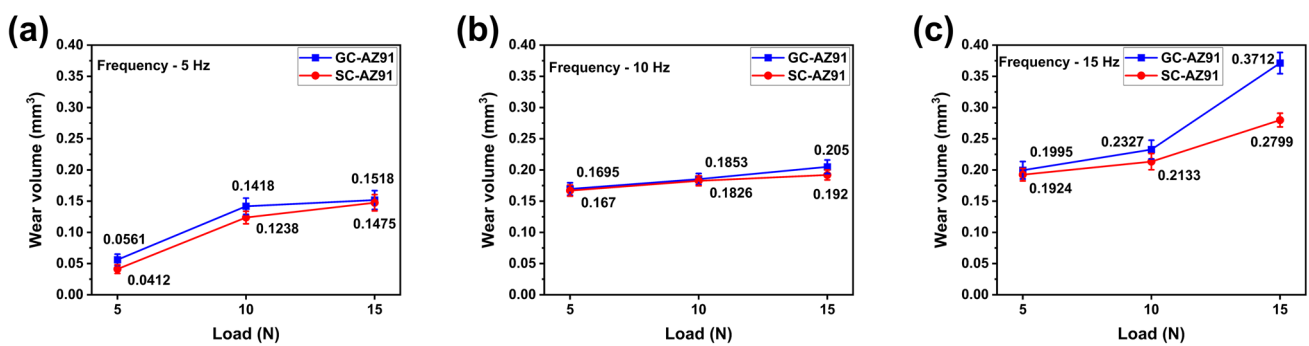


Fig. 12 Effect of variation in loads on the wear volume loss at (a) 5, (b) 10, and (c) 15 Hz oscillating frequency at a constant 200 μm amplitude

Compared to SC AZ91 alloy, in GC AZ91, the higher porosity and higher average grain size (i.e., lesser grain boundary density) translate into a lower yield strength and lower hardness of the GC AZ91 sample. Hence, considering any individual test condition for wear, due to the presence of fewer GBs as obstacles and a higher amount of porosity in the GC AZ91 sample, deeper penetration of the pin and larger wear scar size has been obtained in the present work. Higher casting defects in the GC sample lead to the formation of micro-cracks on the surface during the wear test. A delamination theory has been put out by Waterhouse, Taylor, and Suh to explain how wear spreads through subsurface fractures and results in the separation of substrate plate-like particles [38, 39]. Hence, microcracks in the GC AZ91 sample propagate and result in a delamination of the surface. Thus, delamination and oxidative wear are found to be dominant wear mechanisms for GC AZ91 alloy. Considering the AZ91 Mg alloy, the main wear mechanisms between AZ91 and EN31 tribopair were adhesion, oxidation, abrasion, and delamination, under different fretting conditions.

Conclusion

In the present research work, microstructure, tensile properties and fretting wear behavior were compared for GC AZ91 and SC AZ91 alloy samples. The salient conclusions of this work are summarized as below:

1. Squeeze casting (SC) of AZ91 alloy produced a higher-quality rod with a more uniform microstructure and refined grains, with improvements in YS, UTS, and % elongation of 98.28, 92.6, and 175.0%, respectively, compared to gravity die cast (GC) rod.
2. Increasing oscillating frequency in fretting wear tests resulted in higher COF and wear volume loss in both GC and SC AZ91 alloy due to friction heating and formation of oxide particles. However, with increasing frequency, SC AZ91 exhibited lower COF and better fretting wear resistance compared to GC AZ91 alloy.
3. At higher loading conditions (10 and 15 N), surface asperities got strain-hardened and formed oxides, reduc-

ing friction and achieving steady state quickly which resulted in lower COF. However, wear volume loss increased with applied load due to oxidative wear. With increasing applied load, for all conditions studied in the present work, the SC AZ91 showed better fretting wear resistance compared to the GC AZ91 alloy.

4. Under various fretting circumstances, the dominant wear mechanisms between the AZ91/steel tribopair were adhesion, oxidation, abrasion, and delamination. However, surface oxidation significantly contributed to the increased wear of both GC AZ91 and SC AZ91 alloy samples at higher frequencies (10 and 15 Hz) and higher loading conditions (10 and 15 N).
5. The presence of higher casting defects in the GC AZ91 sample led to the growth of microcracks on the surface, which further propagated, resulting in surface delamination. Consequently, delamination and oxidative wear were found to be more severe in the GC AZ91 sample, leading to a higher wear volume compared to the SC AZ91 sample.

Acknowledgments The author Ankush S. Marodkar would like to thank the Ministry of Education, Government of India for providing a teaching assistantship for doctoral studies. The authors express their gratitude to the Advanced Welding Lab, IIT Indore for providing the facilities for research work.

References

1. B.L. Mordike, K.U. Kainer, *Magnesium alloys and their application* (Wiley, Weinheim, 2000)
2. H. Borkar, M. Hoseini, M. Pkguleryuz, Effect of strontium on the texture and mechanical properties 445 of extruded Mg–1% Mn alloys. *Mater. Sci. Eng. A.* **549**, 168–175 (2012). <https://doi.org/10.1016/j.msea.2012.04.029>
3. D. Eliezer, E. Aghion, F.H. Froes, Magnesium science, technology and applications. *Adv. Perform. Mater.* **5**, 201–212 (1998)
4. B.L. Mordike, T. Ebert, Magnesium properties—applications—potential. *Mater. Sci. Eng. A.* **302**, 37–45 (2001). [https://doi.org/10.1016/S0921-5093\(00\)01351-4](https://doi.org/10.1016/S0921-5093(00)01351-4)
5. A.S. Marodkar, H. Patil, H. Borkar, A. Behl, Effect of squeeze casting and combined addition of calcium and strontium on microstructure and mechanical properties of AZ91 magnesium alloy. *Int. J. Met.* **2023**, 1–19 (2023). <https://doi.org/10.1007/s40962-022-00943-1>
6. F. Aydin, Y. Sun, M.E. Turan, The effect of TiB₂ content on wear and mechanical behavior of az91 magnesium matrix composites produced by powder metallurgy. *Powder Metall. Met. Ceram.* **57**, 564–572 (2019). <https://doi.org/10.1007/s11106-019-00016-9>
7. L. Zhang, Q. Wang, W. Liao, W. Guo, B. Ye, H. Jiang, W. Ding, Effect of homogenization on the microstructure and mechanical properties of the repetitive-upsetting processed AZ91D alloy. *J. Mater. Sci. Technol.* **33**, 935–940 (2017). <https://doi.org/10.1016/j.jmst.2017.01.015>
8. Y. Cubides, A.I. Karayan, M.W. Vaughan, I. Karama, H. Castaned, Enhanced mechanical properties and corrosion resistance of a fine-grained Mg-9Al-1Zn alloy: the role of bimodal grain structure and β -Mg₁₇Al₁₂ precipitates. *Materialia*. **13**, 100840 (2020). <https://doi.org/10.1016/j.mtla.2020.100840>
9. A. Zafari, H.M. Ghasemi, R. Mahmudi, Tribological behavior of AZ91D magnesium alloy at elevated temperatures. *Wear.* **292–293**, 33–40 (2012). <https://doi.org/10.1016/j.wear.2012.06.002>
10. A. Azad, L. Bichler, A. Elsayed, Effect of a novel Al–SiC grain refiner on the microstructure and properties of AZ91E magnesium alloy. *Int. J. Met.* **7**, 49–59 (2013). <https://doi.org/10.1007/BF03355564>
11. I. Gokalp, A. Incesu, Effect of Ca addition to the elevated temperature mechanical properties of AZ series magnesium alloys. *Int. J. Met.* **17**, 1402–1412 (2023). <https://doi.org/10.1007/s40962-022-00872-z>
12. H. Mohammadi, M. Emamy, Z. Hamnabard, The microstructure, mechanical and wear properties of AZ91-x% B4C metal matrix composites in as-cast and extruded conditions. *Mater. Res. Express.* **6**(12), 126522 (2019). <https://doi.org/10.1088/2053-1591/ab5405>
13. A. Afsharnaderi, M. Lotfpour, H. Mirzadeh, M. Emamy, M. Malekan, Enhanced mechanical properties of as-cast AZ91 magnesium alloy by combined RE-Sr addition and hot extrusion. *Mater. Sci. Eng. A.* **792**, 139817 (2020). <https://doi.org/10.1016/j.msea.2020.139817>
14. Y. Zhang, G. Wu, W. Liu, L. Zhang, S. Pang, Y. Wang, W. Ding, Effects of processing parameters and Ca content on microstructure and mechanical properties of squeeze casting AZ91–Ca alloys. *Mater. Sci. Eng. A.* **595**, 109–117 (2014). <https://doi.org/10.1016/j.msea.2013.12.014>
15. H. Hu, Squeeze casting of magnesium alloys and their composites. *J. Mater. Sci.* **33**, 1579–1589 (1998)
16. F. Pan, M. Yang, X. Chen, A review on casting magnesium alloys: modification of commercial alloys and development of new alloys. *J. Mater. Sci. Technol.* **32**, 1211–1221 (2016). <https://doi.org/10.1016/j.jmst.2016.07.001>
17. P.I. Hurricks, The mechanism of fretting—a review. *Wear.* **16**, 389–409 (1970). [https://doi.org/10.1016/0043-1648\(70\)90235-8](https://doi.org/10.1016/0043-1648(70)90235-8)
18. D.S. Mehta, S.H. Masood, W.Q. Song, Investigation of wear properties of magnesium and aluminum alloys for automotive applications. *J. Mater. Process. Technol.* **155–156**, 1526–1531 (2004). <https://doi.org/10.1016/j.jmatprotec.2004.04.247>
19. N.N. Aung, W. Zhou, L.E.N. Lim, Wear behaviour of AZ91d alloy at low sliding speeds. *Wear.* **265**, 780–786 (2008). <https://doi.org/10.1016/j.wear.2008.01.012>
20. D. Khabale, M.F. Wani, Tribological characterization of AZ91 and AE42 magnesium alloys in fretting contact. *J. Tribol.* **140**, 011604 (2018). <https://doi.org/10.1115/1.4036922>
21. H. Weijiu, Z. Rongchang, C. Anhu, A comparative study on the fretting wear resistant properties of AZ91D and AM60B magnesium alloys. *Mater. Sci. Forum.* **488–489**, 745–748 (2005). <https://doi.org/10.4028/www.scientific.net/MSF.488-489.745>
22. R. Ramesh, R. Gnanamoorthy, Effect of hardness on fretting wear behaviour of structural steel, En 24, against bearing steel, En 31. *Mater. Des.* **28**, 1447–1452 (2007). <https://doi.org/10.1016/j.matdes.2006.03.020>
23. J.A. Halling, Crossed-cylinder wear machine and its use in the study of severe wear of brass on mild steel. *Wear.* **4**, 22–31 (1961)
24. K. Sikdar, S. Shekhar, K. Balani, Fretting wear of Mg–Li–Al based alloys. *Wear.* **318**, 177–187 (2014). <https://doi.org/10.1016/j.wear.2014.06.012>
25. A.K.S. Bankoti, A.K. Mondal, S. Kumar, B.C. Ray, Individual and combined additions of calcium and antimony on microstructure and mechanical properties of squeeze-cast AZ91D magnesium alloy. *Mater. Sci. Eng. A.* **626**, 186–194 (2015). <https://doi.org/10.1016/j.msea.2014.12.068>

26. R. Ramesh, R. Gnanamoorthy, Fretting wear behavior of liquid nitrided structural steel, En24 and Bearing Steel, En31. *J. Mater. Process. Technol.* **171**, 61–67 (2006). <https://doi.org/10.1016/j.jmatprotec.2005.06.048>
27. M. Horynová, J. Zapletal, P. Doležal, P. Gejdoš, Evaluation of fatigue life of AZ31 magnesium alloy 518 fabricated by squeeze casting. *Mater. Des.* **45**, 253–264 (2013). <https://doi.org/10.1016/j.matdes.2012.08.079>
28. T.M. Yue, H. Ha, N. Musson, Grain size effects on the mechanical properties of some squeeze cast light alloys. *J. Mater. Sci.* **30**, 2277–2283 (1995). <https://doi.org/10.1007/BF01184573>
29. M. Masoumi, H. Hu, Influence of applied pressure on microstructure and tensile properties of squeeze cast magnesium Mg–Al–Ca alloy. *Mater. Sci. Eng. A.* **528**, 3589–3593 (2011). <https://doi.org/10.1016/j.msea.2011.01.032>
30. S. Kleiner, O. Beffort, A. Wahlen, P. Uggowitzer, Microstructure and mechanical properties of squeeze cast and semi-solid cast Mg–Al alloys. *J. Light Met.* **2**, 277–280 (2002). [https://doi.org/10.1016/S1471-5317\(03\)00012-9](https://doi.org/10.1016/S1471-5317(03)00012-9)
31. Y. Cubides, A.I. Karayan, M. Vaughan, I. Karaman, H. Castaneda, Enhanced mechanical properties and corrosion resistance of a fine-grained Mg–9Al–1Zn alloy: the role of bimodal grain structure and β -Mg₁₇Al₁₂ precipitates. *Materials*. **13**, 100840 (2020). <https://doi.org/10.1016/j.mtla.2020.100840>
32. Y. Zhang, G. Wu, W. Liu, L. Zhang, S. Pang, Y. Wang, W. Ding, Effects of processing parameters and Ca content on microstructure and mechanical properties of squeeze casting AZ91–Ca alloys. *Mater. Sci. Eng. A.* **595**, 109–117 (2014). <https://doi.org/10.1016/j.msea.2013.12.014>
33. J. Bai, Y. Sun, F. Xue, J. Qiang, Microstructures and creep properties of Mg–4Al–(1–4) La alloys produced by different casting techniques. *Mater. Sci. Eng. A.* **552**, 472–480 (2012). <https://doi.org/10.1016/j.msea.2012.05.072>
34. H. Yu, S. Chen, W. Yang, Y. Zhang, S. Chen, Effects of rare element and pressure on the microstructure and mechanical property of AZ91D alloy. *J. Alloys Compd.* **589**, 479–484 (2014). <https://doi.org/10.1016/j.jallcom.2013.12.019>
35. L.A. Dobrzanski, T. Tanski, L. Cizek, J. Domagała, Mechanical properties and wear resistance of magnesium casting alloys. *J. Achiev. Mater. Manuf. Eng.* **31**(1), 83–90 (2008)
36. G.E. Dieter, *Mechanical metallurgy, SI metric* (McGraw-Hill, London, 1988)
37. U. Bryggman, S. Sodenberg, Contact conditions and surface degradation mechanisms in low amplitude fretting. *Wear*. **125**, 39–52 (1988)
38. N.P. Suh, The delamination theory of wear. *Wear*. **25**, 111 (1973)
39. R.B. Waterhouse, D.E. Taylor, Fretting debris and the delamination theory of wear. *Wear*. **29**, 337–344 (1974)

Publisher's Note Springer Nature remains neutral with regard to jurisdictional claims in published maps and institutional affiliations.

Springer Nature or its licensor (e.g. a society or other partner) holds exclusive rights to this article under a publishing agreement with the author(s) or other rightsholder(s); author self-archiving of the accepted manuscript version of this article is solely governed by the terms of such publishing agreement and applicable law.